J Solid State Electrochem (2001) 5: 131–140 © Springer-Verlag 2001

ORIGINAL PAPER

Ermete Antolini · Leonardo Giorgi
Francesco Cardellini · Enza Passalacqua

Physical and morphological characteristics and electrochemical behaviour in PEM fuel cells of PtRu/C catalysts

Received: 2 December 1999 / Accepted: 27 January 2000

Abstract Platinum-ruthenium catalysts supported on carbon (PtRu/C) have been characterized by X-ray diffraction (XRD), transmission electron microscopy (TEM), specific surface area analysis (BET), X-ray photoelectron spectroscopy (XPS) and in proton exchange membrane (PEM) fuel cell tests. The results indicate the presence of strong metal-carbon interactions, which hinder the formation of a single-phase face-centered cubic (fcc) PtRu alloy. The particle size of the PtRu/C catalysts was smaller than both carbon-supported platinum (Pt/C) and ruthenium (Ru/C) catalysts. In the bimetallic electrocatalysts the intercrystallite distance decreased with respect to pure Pt and Ru metals. PEM fuel cell tests in H_2/air operation mode revealed a decrease of performance with increasing carbon content of the catalyst, at a fixed Pt loading. In H_2 + 100 ppm CO/air operation mode the maximum performance of the PEM fuel cell was attained at 0.63 atomic fraction Ru.

Key words Platinum · Ruthenium · Carbon-supported catalysts · Polymer electrolyte fuel cell · Carbon monoxide oxidation

E. Antolini · L. Giorgi
ENEA C.R. Casaccia, Erg Tea Echi,
Via Anguillarese 301,
00060 Santa Maria di Galeria (Rome), Italy
e-mail: antolinie@casaccia.enea.it
Tel.: +39-6-30486552; Fax: +39-6-30486357

F. Cardellini
ENEA C.R. Casaccia, Inn Numa Matav, Via Anguillarese 301,
00060 Santa Maria di Galeria (Rome), Italy

E. Passalacqua
CNR, Institute for Transformation and Storage of Energy,
Via Salita S. Lucia sopra Contesse 39,
98126 S. Lucia, Messina, Italy

Present address:
E. Antolini (✉)
Scuola di Scienza dei Materiali, Via 25 Aprile 22,
16016 Cogoleto (Genova), Italy
e-mail: ermantol@libero.it
Tel.: 010 918 2880; Fax: 010 918 2368

Introduction

It is well known that platinum is the best electrocatalyst for hydrogen oxidation. Hydrogen/oxygen proton exchange membrane (PEM) fuel cells are highly attractive as power sources for mobile applications, since they operate at a relatively low temperature (about 80 °C) which is advantageous for rapid cell start-up. To be competitive, PEM fuel cells must operate by the reforming of natural gas or liquid hydrocarbons, as methanol [1]. Reformed fuel gas mixtures contain carbon monoxide, a severe poison for Pt, which leads to a decrease of fuel cell performance [2]. CO poisoning is caused by chemisorption of CO onto Pt electrocatalysts, forming a nearly complete CO monolayer which blocks sites for electrooxidation of hydrogen. H_2 oxidation becomes severely polarized as the monolayer approaches complete coverage. This polarization can be reduced by removing a small fraction of the CO from the Pt surface [3]. To improve CO tolerance of fuel cell anodes, several bimetallic Pt-based electrocatalysts have been proposed, such as PtSn [4–6], PtRu [7–10] and PtMo [11, 12]. PtRu alloy catalysts represent the state of the art for anodes operating on reformed gas mixtures [13]. To achieve lower CO coverage values, two types of mechanism have been proposed. An intrinsic mechanism postulates that the presence of Ru modifies H_2 and CO chemisorption properties, so as to reduce CO coverage with respect to H_2 oxidation sites [14]. A promoted mechanism is based on CO oxidation at low potentials. In order to oxidize an adsorbed CO molecule, a neighbouring site is needed for adsorption of water. The increased reactivity with respect to CO oxidation observed on PtRu alloys can be understood in terms of the lower oxidation potential for the Ru atoms compared to Pt, leading to preferential chemisorption of water:

$$\mathrm{Ru} + \mathrm{H_2O} \rightarrow \mathrm{Ru\text{-}OH} + \mathrm{H^+} + \mathrm{e^-} \quad (1)$$

Previous work reported that the best activity observed for CO oxidation was found for a PtRu alloy

having a bulk Pt:Ru atomic ratio of 1:1 [15–17]. The fact that 1:1 Pt:Ru showed the lowest CO oxidation potential supports a bifunctional mechanism [7] according to:

$$\text{Ru-OH} + \text{Pt-CO} \rightarrow \text{Ru} + \text{Pt} + \text{CO}_2 + \text{H}^+ + \text{e}^- \qquad (2)$$

where Ru adsorbs the oxygen-containing species and CO binds to Pt. CO adsorption is equally facile at Pt-Pt, Ru-Ru and Pt-Ru sites, but a reduced adsorption strength of OH on Pt-Ru pairs was suggested by Gasteiger et al. [18], who said that for a composition of 50% PtRu the number of Pt-Ru sites is maximized. In the aforementioned reports the maximum Ru content in the alloy was 50 at%. To investigate the behaviour of PtRu alloys for compositions with Pt/Ru < 1, in the present work we have also studied a Pt:Ru composition of 1:3.

The effect of the carbon support on the PtRu alloy phase composition and surface area is also important. The difference between model catalysts (bimetallic alloys of known surface composition) and real catalysts (supported bimetallics) is due to the presence of metal-supported electronic effects. The properties and catalytic behaviour of this kind of catalyst depend partly on the type of supported metal and the porosity and purity of the support [19, 20], but there is also a strong effect of the surface chemistry of the carbon material [21]. In fact, taking into account the hydrophobic character of the carbon, the presence of oxidized complexes on its surface could modify the wettability properties during the impregnation of the support with the metal precursors in polar media [22]. Moreover, the modification of the surface chemistry of the carbon by activation treatments can produce a noticeable effect in the metal precursor-support interaction [23–25]. The beneficial effects of the activation treatments on the catalytic properties appear to depend on the type and the amount of the complexes developed on the carbon surface [25]. Generally, both bulk and supported PtRu alloys are prepared starting from the same precursors, H_2PtCl_6 and $RuCl_3$. However, unlike unsupported PtRu, previous work has indicated that it is difficult to obtain single-phase PtRu/C alloy. Rauhe et al. [26], starting from a nominal Pt:Ru composition of 1:1 deposited on graphitized carbon, obtained pure Pt and a Ru-rich alloy. He et al. [27], starting from a nominal Pt:Ru composition of 1:1 on high surface carbon, obtained a Ru atomic fraction of 0.2 in the PtRu alloy, with some Ru present in an amorphous form. Finally, McBreen and Mukerjee [28], starting from an atomic ratio of Ru to Pt of 3.4:1 on carbon, found a large excess of unalloyed Ru, with only about 10% of the Ru alloyed with the Pt.

Optimization of the PtRu/C electrocatalyst composition and morphology is very important for the future development of PEM fuel cells. The aim of this work is to evaluate the effect of Ru content on carbon-supported PtRu alloys with respect to phase composition, crystallinity, particle size and surface area of the alloy and metal-carbon interaction, and to correlate them to fuel cell performance with H_2 and H_2 + CO. In this work, particular attention was focused on the effect of the Ru content in the alloy on the thickness of the catalyst layer of the PEM fuel cell anodes at a fixed platinum loading.

Experimental

The carbon-supported PtRu catalysts of various Pt:Ru atomic ratios and Me/C = Me/(Me + C) weight ratios (Me = Pt + Ru) were supplied from E-TEK (Natick, Mass., USA), to our specifications. All PtRu alloys were supported on carbon Vulcan XC-72 (surface area 250 $m^2\ g^{-1}$). The preparation method of the catalyst, by a deposition and reduction process of Pt and Ru precursors, has been described by Radmilovic et al. [29]. The powders were fabricated by a spray technique into a three-layer electrode for PEM fuel cells [30]. The porous electrodes comprised a carbon paper support (Toray TGPH090), a polytetrafluoroethylene (PTFE)-bonded carbon (Vulcan XC-72) diffusion layer deposited onto the carbon support, and a Nafion-bonded Pt/C (cathode and reference anode) or PtRu/C (anode) catalyst layer deposited onto the diffusion layer. The platinum loading of the cathode and the reference anode was 0.1 mg cm^{-2}. The platinum loading of the PtRu/C anode was maintained constant at about 0.6 mg cm^{-2}, while the total metal loading changed with the alloy used. As a consequence, the thickness of the catalyst layer increases with Ru content in the catalyst powder (see later). The ratio between catalyst loading and Nafion loading was kept constant for all the electrodes at 3:1. The membrane/electrode assemblies (MEAs) were prepared by hot-pressing the electrodes onto the Nafion 117 membrane at 130 °C for 3 min. The MEAs performance was evaluated in a 50 cm^2 single cell (Globe Tech) in both a H_2/air operation mode (H_2 op) and a H_2 + 100 ppm CO/air operation mode (CO op).

X-ray diffraction (XRD) measurements were carried out with a Italstructures powder diffractometer, using a focused and monochromatized Co K_α source, with a position-sensitive detection of 120°.

X-ray photoelectron spectroscopy (XPS) measurements were performed using a V.G. Escalab MKII spectrometer, with an Al K_α X-ray source (1486.6 eV).

The Brunauer, Emmett and Teller (BET) specific surface area of the catalyst powders was measured with a Nova 2000 Quantacrome surface area analyser.

Transmission electron microscope (TEM) analyses were performed using a TEM JEOL 4000FX operating at an acceleration voltage up to 400 kV.

The cell potential versus current density measurements were recorded using a computer interfaced with a fuel cell test-station (Globe Tech). Experimental measurements were carried out at 70 and 90 °C, at an absolute pressure of 2.5 bar for the anode side and 3 bar for the cathode side. The gas fluxes were fixed at 1.5 times stoichiometric for the fuel and 3 times stoichiometric for the air at a current density of 1 A cm^{-2}.

Results and discussion

Phase composition and lattice parameters

XRD is a bulk method, and reveals information on the bulk structure of the catalyst and its support. XRD patterns of carbon-supported Pt, Ru and their alloy electrocatalysts are shown in Fig. 1 (Me/C = 20%, various Pt:Ru ratios) and Fig. 2 (Pt:Ru = 1:1, various Me/C). The first peak is associated with the carbon support. The Pt pattern displays the (111), (200), (220) and (311) reflection characteristics of a face-centred

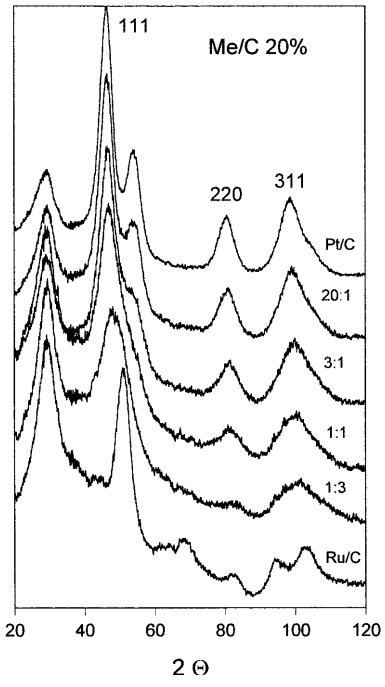

Fig. 1 X-ray diffraction patterns of carbon-supported Pt, PtRu and Ru samples, at a fixed Me/C of 20%

cubic (fcc) crystal structure. The Ru pattern displays the reflection characteristics of its hexagonal close-packed (hcp) crystal structure. In the bulk alloys, for a Ru atomic fraction up to 0.62, Pt and Ru can form a solid solution with Ru atoms replacing Pt atoms in a fcc structure. Above 0.62 Ru atomic fraction, another solid solution is formed in which the Ru atoms are replaced by Pt atoms in an hcp structure. Using XRD one can determine the composition of the alloy by the shift of the Pt reflections, i.e. by the variation of the crystal lattice, as in Vegard's law. Figure 3 shows the dependence of the lattice constant of the fcc structure on Ru content for the samples with a Me/C ratio of 20%. Lattice constants were calculated from the reflections (220) and (311). For comparison, the dependence of the lattice constant of the unsupported bulk alloy is also shown (dashed line, data from [31] and [32]). The value of the Pt/C lattice constant was slightly lower than unsupported Pt, likely owing to platinum-carbon interactions. Up to the composition of Pt:Ru = 3:1 the decrease of the lattice constant of the carbon-supported sample with increasing Ru content was similar to the unsupported solid solution, indicating the formation of an alloy with a fcc structure. The lattice constant for the composition Pt:Ru = 1:1, instead, deviated from linearity and its value was almost similar to the Pt:Ru = 3:1 sample. The pattern of this sample also revealed the reflections of the hcp structure, indicating the presence of a Ru-rich alloy. The amount of the hcp structure increased in the Pt:Ru = 1:3 sample. In Fig. 4 can be seen the dependence of the lattice constant of the fcc structure on the Me/C ratio, at fixed composition Pt:Ru = 1:1. On increasing the Me/C ratio, the hcp phase disappeared and the composition of the fcc alloy approached the nominal value of Pt:Ru = 1:1.

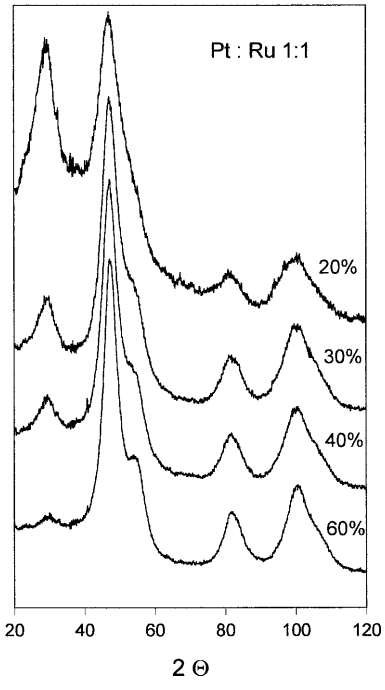

Fig. 2 X-ray diffraction patterns of PtRu/C catalysts with Pt:Ru = 1:1 at various Me/C ratios

Particle size by XRD and TEM

The best techniques to determine the particle size of carbon-supported PtRu catalysts are XRD and TEM. The use of cyclic voltammetry to determine the hydrogen adsorption area of the catalyst is not feasible for ruthenium owing to overlap of the hydrogen adsorption and oxygen adsorption potentials and the tendency of hydrogen to absorb in the ruthenium lattice [33]. Using the BET analysis, instead we measure the surface area of both the support and the catalyst.

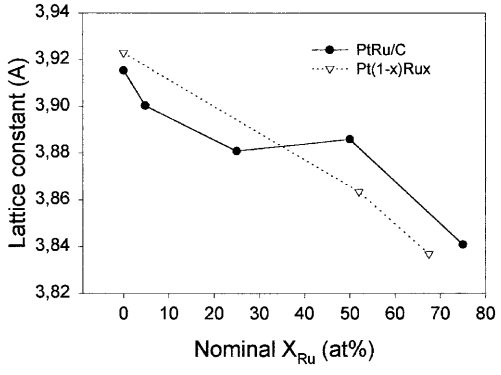

Fig. 3 Dependence of fcc lattice constant on Ru content of the samples at Me/C = 20%. The *dashed line* refers to PtRu bulk alloys (from [31] and [32]). Lattice constant error ±0.001 Å

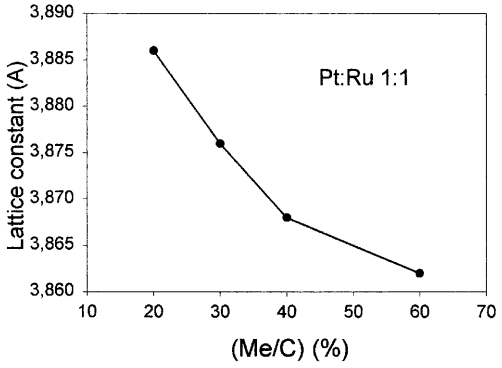

Fig. 4 Dependence of fcc lattice constant on Me/C ratio for PtRu/C catalysts with Pt:Ru = 1:1 (lattice constant error ±0.001 Å)

X-ray diffraction

The average particle sizes and surface areas of the catalysts can be estimated from the broadening of the (220) reflection for Pt/C and PtRu/C and the (101) reflection for Ru/C by means of the following equations:

$$D = k\lambda/\beta\cos\theta \tag{3}$$

$$SA = 60,000/\rho D \tag{4}$$

where D is the mean particle size in Å, k is a coefficient taken here as 0.9, λ the wavelength of the X-rays used (1.789 Å), β the width of the diffraction peak at half height, θ the angle at the position of the peak maximum, SA the surface area ($m^2\ g^{-1}$), and ρ the density (21.4 g cm^{-3} for Pt, 12.3 g cm^{-3} for Ru). The alloy density is, to a good approximation:

$$\rho_{PtRu} = y_{Pt}\rho_{Pt} + y_{Ru}\rho_{Ru} \tag{5}$$

where y_{Pt} and y_{Ru} are the mass fractions of platinum and ruthenium, respectively. The particle sizes of carbon-supported Pt, PtRu and Ru are listed in Table 1. The particle size of the PtRu samples was lower than both pure Pt and Ru. In Fig. 5 the dependence of surface area on Ru content of the samples at a fixed Me/C of 20% is shown. The specific surface area of the samples showed a maximum for the composition Pt:Ru = 1:3, according to the results of Chu and Gilman [32] for unsupported alloys. Figure 6 shows the particle size dependence (particle size values from E-TEK) for Pt:Ru = 1:1 and for Pt alone on metal moles per unit mass of carbon, calculated from the following relations:

$$\text{Pt/C: mol Pt(g C)}^{-1} = (\text{Me/C})/M_{Pt}[1 - (\text{Me/C})] \tag{6}$$

$$\text{PtRu/C: mol(Pt + Ru)(g C)}^{-1} = 2/(1 + M_{Ru}/M_{Pt})(\text{Me/C})/M_{Pt}[1 - (\text{Me/C})] \tag{7}$$

where M_{Pt} and M_{Ru} are the atomic weights of Pt and Ru, respectively. As can be seen, while the particle size of the Pt samples increased with the number of platinum moles in a remarkable way, the particle size of the Pt:Ru = 1:1 samples only slightly increased with the number of metal moles. The presence of Ru seems to hinder the growth of the particles, so allowing a better dispersion of the metals. This behaviour should depend on the different mechanisms for the impregnation/reduction processes for the Pt and Ru precursors alone and for Pt and Ru when the precursors are mixed together. Table 2 shows the values of the (Pt + Ru) atom number in PtRu/C (Na_{PtRu}) to the Pt atom number in Pt/C (Na_{Pt}) per metal particle, at a fixed Me/C value of 20%, obtained by the relation:

Table 1 Particle size of Pt/C, PtRu/C and Ru/C catalysts obtained from XRD and TEM measurements

Sample	XRD (nm)	TEM (nm)
20%, Pt	2.4	2.6
20%, PtRu = 20:1	2.15	–
20%, PtRu = 3:1	1.95	1.9
20%, PtRu = 1:1	1.75	2.1
20%, PtRu = 1:3	1.6	2.1
20%, Ru	2.9	2.8
30%, PtRu = 1:1	1.85	–
40%, PtRu = 1:1	2.0	–
60%, PtRu = 1:1	2.1	–

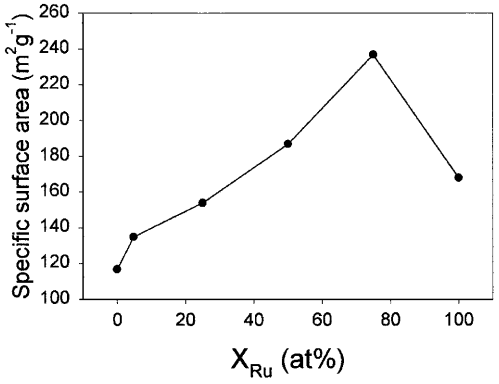

Fig. 5 Specific surface area from XRD measurements versus Ru content of the catalysts, at Me/C = 20%

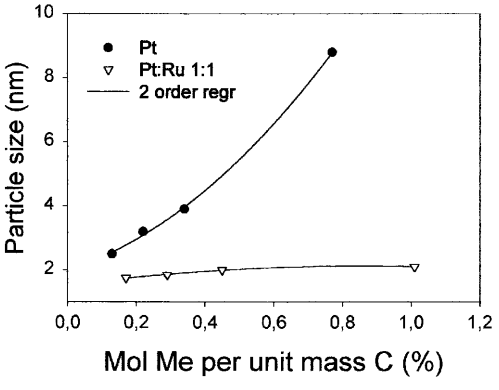

Fig. 6 Particle size dependence on metal moles per unit mass of carbon for Pt/C and PtRu/C with Pt:Ru = 1:1

Table 2 Values of the ratio of the (Pt + Ru) atom number per metal particle in PtRu/C to Pt atom number per metal particle in Pt/C (Na_{PtRu}/Na_{Pt}), and of the ratio of the PtRu crystallite number in PtRu/C to Pt crystallite number in Pt/C (Nc_{PtRu}/Nc_{Pt}). Mean values from particle size by XRD and TEM

Sample	Na_{PtRu}/Na_{Pt}	Nc_{PtRu}/Nc_{Pt}
Pt	1	1
PtRu = 3:1	0.49	2.3
PtRu = 1:1	0.51	2.6
PtRu = 1:3	0.51	3.1
Ru	1.66	1.15

$$Na_{PtRu}/Na_{Pt} = (D_{PtRu}/D_{Pt})^3 \rho_{PtRu}/\rho_{Pt} M_{Pt}/M_{PtRu} \quad (8)$$

where D_{Pt} and D_{PtRu} are the grain sizes of Pt and PtRu, ρ_{Pt} and ρ_{PtRu} are the densities of Pt and PtRu, and M_{PtRu} is the average molecular weight of the PtRu samples, as $M_{PtRu} = x_{Ru}M_{Ru} + (1 - x_{Ru})M_{Pt}$, with x_{Ru} the molar fraction of Ru. The number of atoms per metal particle in PtRu/C catalysts was less than 0.5 with respect to Pt/C and less than 0.3 with respect to Ru/C.

Transmission electron microscopy

From the TEM images, Pt clusters appeared uniformly distributed in the carbon support. Figure 7a–e shows the distribution of particle size for Pt/C, PtRu/C and Ru/C catalysts. For all the samples, particle size distribution was monomodal. The particle size distribution of bimetallic catalysts was narrower than that of monometallic Pt/C and Ru/C. From the comparison of particle sizes listed in Table 1, we can note a good agreement of the values obtained from the TEM and XRD analyses.

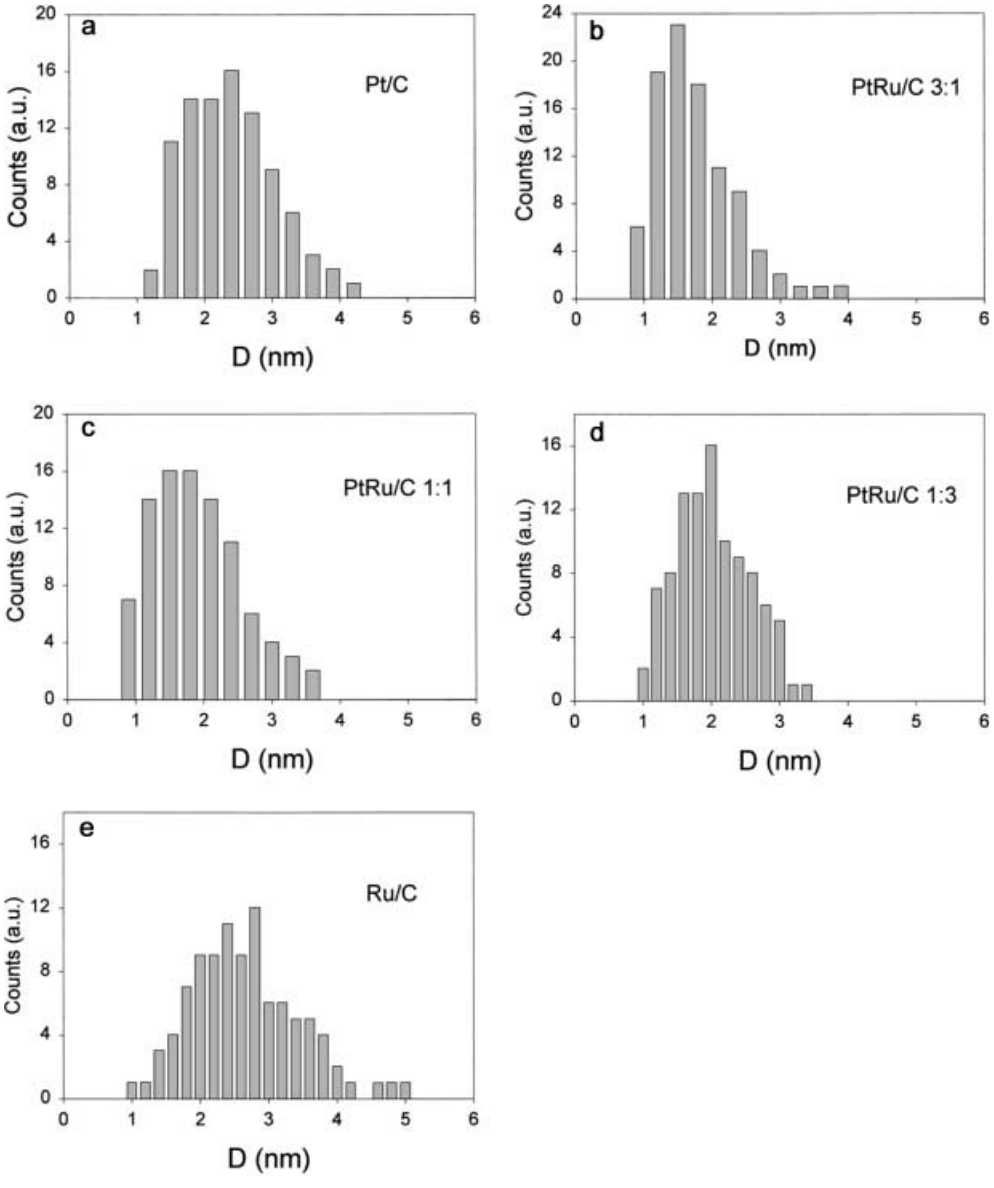

Fig. 7 Particle size distribution from TEM measurements for Pt/C (**a**), PtRu/C with Pt: Ru = 3:1 (**b**), 1:1 (**c**), 1:3 (**d**) and Ru/C (**e**)

BET analysis

In the case of unsupported alloys, the specific surface area can be measured using nitrogen physisorption and BET analysis. For supported alloys, one needs a selectively adsorbing probe molecule, that adsorbs on the alloy atoms but not the support atoms. Using N_2, the total specific surface area can be obtained by the following relationship:

$$SA_{\mathrm{BET}} = SA_{\mathrm{C}}(1-y) + SA_{\mathrm{Me}}y - k[SA_{\mathrm{C}}(1-y)SA_{\mathrm{Me}}y]^{0.5} \quad (9)$$

where SA_{BET} is experimental specific surface area, SA_{C} and SA_{Me} are the specific surface areas of carbon and total metal, respectively, y is the mass fraction of the total metal, and k is a carbon-metal interaction parameter. The values of SA_{BET} are given in Table 3. Unfortunately, k is unknown, so we cannot obtain the value of SA_{Me}. However, inserting in Eq. 9 the value of SA_{Me} from XRD, from all samples we can determine the value of k. The values of k for the PtRu samples were slightly higher (5–10%) than the value of k for pure Pt (see Table 3), so indicating a stronger carbon-metal interaction for the PtRu samples with respect to pure Pt.

Mean intercrystallite distance

The interparticle separation is an important characteristic of the catalyst, as indicated by parallel studies on oxygen reduction on platinum particles, where it was found that small intercrystallite distances result in lower activity [34]. The mean intercrystallite distance for Pt and PtRu was calculated by the following equation, proposed by Watanabe et al. [35]:

$$x_i = (1/3)[(3)^{0.5}\pi\rho D^3 SA_{\mathrm{C}}(1-y)/y]^{0.5} \quad (10)$$

where x_{i} is mean intercrystallite distance, ρ and D are the density and the particle size of the metal, SA_{C} the specific surface area of the carbon and y the metal content of Me/C. Figure 8 shows x_{i} versus Ru content in PtRu samples at a fixed Me/C value of 20%. The intercrystallite distance for PtRu compositions is shorter than that for pure Pt and pure Ru, with a minimum for Pt:Ru = 1:3. Figure 9 shows the dependence of the interparticle distance for Pt alone and for PtRu = 1:1 on metal moles per unit mass of carbon. The intercrystallite distance for Pt alone increases with increasing platinum moles, while for PtRu the value of x_{i} slightly decreases with increasing metal moles. In the absence of Ru precursors, Pt precursors are preferentially adsorbed where they were deposited before, and as a consequence they increase in size more than in the case of PtRu compositions. For PtRu/C samples, we suppose that in the first stage of deposition the Pt and Ru precursors are preferentially adsorbed onto different C sites. This should explain both the decrease of the intercrystallite distance with respect to Pt alone and Ru alone, and the formation of both fcc and hcp structures, as revealed by XRD. Table 2 shows the values of the PtRu crystallite number in PtRu/C (Nc_{PtRu}) to the Pt crystallite number in Pt/C (Nc_{Pt}) per unit mass of carbon, at a fixed Me/C ratio, calculated by the relation:

$$Nc_{\mathrm{PtRu}}/Nc_{\mathrm{Pt}} = 1/[(D_{\mathrm{PtRu}}/D_{\mathrm{Pt}})^3 \rho_{\mathrm{PtRu}}\rho_{\mathrm{Pt}}] \quad (11)$$

The number of crystallites in the PtRu/C catalysts was about 2.5 times higher than that for both Pt/C and Ru/C.

Table 3 Specific surface area values from BET measurements and carbon-metal interaction parameter (k) values, obtained by inserting in Eq. 9 the values of the specific surface area from XRD

Sample	SA from BET ($m^2\ g^{-1}$)	k
20%, Pt	153.5	1.02
20%, PtRu = 3:1	144.8	1.10
20%, PtRu = 1:1	144.0	1.08
20%, PtRu = 1:3	143.2	1.07
40%, PtRu = 1:1	103.2	1.13

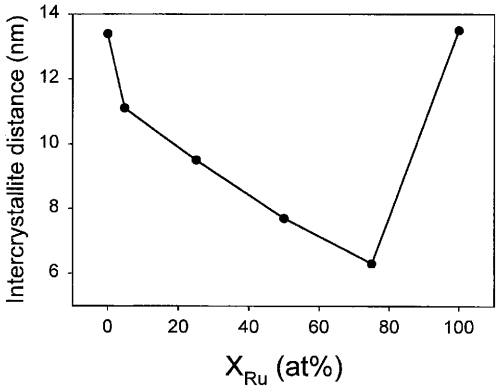

Fig. 8 Mean intercrystallite distance as a function of Ru content of the samples

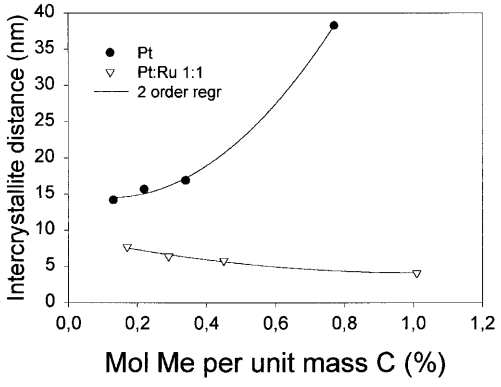

Fig. 9 Mean intercrystallite distance as a function of mol Me per unit mass of carbon for Pt/C and PtRu/C with Pt:Ru = 1:1

XPS analysis

Normally, one thinks of XPS as a surface-sensitive technique, and that is true for non-porous solids, but for porous solids like supported metal catalysts the XPS spectra come from the whole crystallite, since the crystallite size is typically of the same order of magnitude as the escape depth of the photoelectrons. No information can be obtained by investigation of the Ru 3d signal, because of interference from the carbon support (the C 1s signal). Figure 10 shows the Pt 4f spectra of bulk Pt and of Pt/C and PtRu/C catalysts. For the Pt/C catalyst, the peak maximum for the Pt $4f_{7/2}$ shifted to higher values by 0.4 eV with respect to unsupported platinum, according to previous studies on zeolite-supported [36] and carbon-supported [37] platinum. This was interpreted as being due to the presence of a platinum-support electronic effect. The specific metal-support interaction is through electron transfer from platinum clusters to oxygen atoms of the surface of the support. The metal-support interaction is considered to be beneficial to the enhancement of catalytic properties [36] and to improved stability of the electrocatalyst [38]. It is realized that when two solids are joined to form an adhesive couple, the adhesion properties of the couple depend on the morphological, chemical and physical nature of their interface [39]. In the absence of material mixing and mechanical interlocking, the adhesion is intrinsic in nature and arises from molecular, electrostatic or chemical surface forces acting across the interface of two dissimilar substances. In many cases, chemical bonds are formed or charge transfer takes place between the contacting phases. There is also a small-particle effect [40–43]: particles in the 1–2 nm range have not yet attained the normal bulk band structure, so the binding energy for the particles shifts to higher values, the full width at half maximum (FWHM) of the peak increases, and its intrinsic asymmetry decreases relative to the bulk metal. Unlike the result of Shukla et al. [44], for PtRu/C catalysts a further shift to higher values for the Pt $4f_{7/2}$ by 0.2–0.3 eV was observed. This further shift for the PtRu/C samples should be related (1) to different oxidation states of the platinum, or (2) to metal–metal interactions, or (3) to metal-support interactions or (4) small cluster-size effects. The Pt 4f spectra of Pt/C and PtRu/C samples have been deconvoluted into three doublets of the same binding energy (same components) and intensity (same amounts), indicating the absence of different Pt oxidation states. Denis et al. [45] found the Pt 4f signal for a carbon-supported PtRu composition in the ratio 1:1 slightly shifted towards lower binding energies with respect to unsupported Pt. On this basis, the shift towards higher binding energies for Pt 4f spectra of PtRu/C samples with respect to Pt/C is due to stronger platinum-carbon interactions or small-particle effects. The presence of Ru precursors and their decomposition can influence the acid-base properties of the carbon support. This effect can produce a strong metal-support interaction, which affects the electronic nature of the platinum sites.

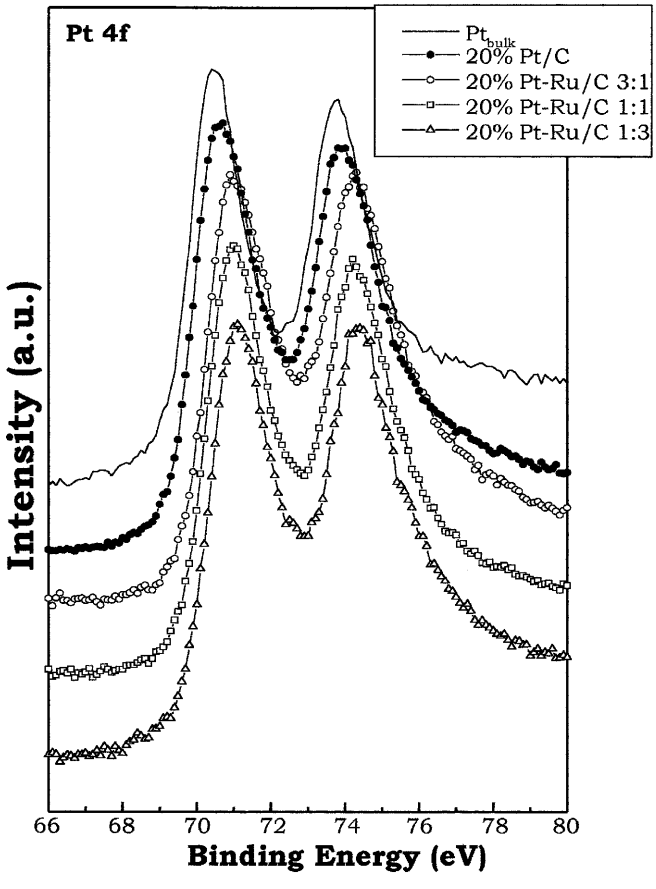

Fig. 10 Pt 4f X-ray photoelectron spectra of Pt metal, Pt/C and PtRu/C of different compositions

C/Pt ratio

The mass of carbon per unit mass of platinum (C/Pt) for the PtRu/C catalyst depends on the Ru/Pt atomic ratio and Me/C in the following way:

$$(\mathrm{C/Pt}) = [1/(\mathrm{Me/C}) - 1](1 + \alpha M_{\mathrm{Ru}}/M_{\mathrm{Pt}}) \quad (12)$$

where α is the Ru/Pt atomic ratio, and M_{Ru} and M_{Pt} are the atomic mass of Ru and Pt, respectively. At a fixed Pt loading of the anode, the carbon amount of the catalyst layer linearly increases with α and decreases with increases in Me/C. The thickness d of the catalyst layer is:

$$d = V/S \quad (13)$$

where S is the geometric area of the electrode and V is the volume of the layer. The total volume of the layer is the sum of the volumes of the components of the layer:

$$V = V_{\mathrm{Pt}} + V_{\mathrm{C}} + V_{\mathrm{Ru}} + V_{\mathrm{N}} \quad (14)$$

where V_{Pt}, V_{C}, V_{Ru} and V_{N} are the volumes of Pt, C, Ru and Nafion in the catalyst layer, respectively. Since $V = m/\rho$, from Eqs. 12, 13, 14 we obtain:

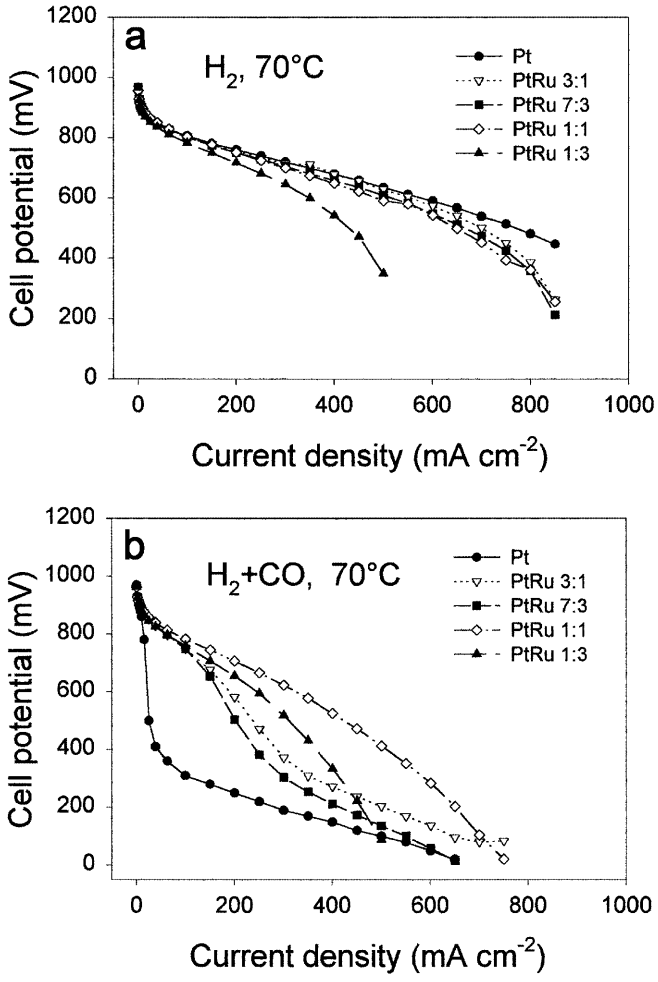

Fig. 11 Cell voltage versus current density at 70 °C in H_2 op (**a**) and H_2 + CO op (**b**) for Pt/C and PtRu/C catalysts as anodes, at Me/C = 20%

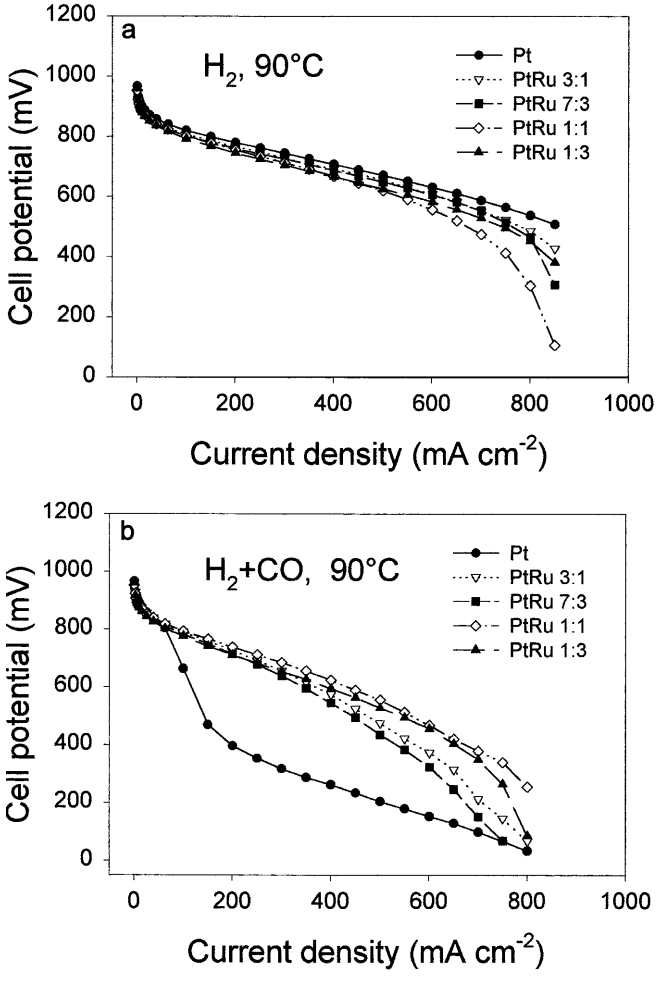

Fig. 12 Cell voltage versus current density at 90 °C in H_2 op (**a**) and H_2 + CO op (**b**) for Pt/C and PtRu/C catalysts as anodes, at Me/C = 20%

$$d = m_{\mathrm{Pt}}/S\{1/\rho_{\mathrm{Pt}} + (\mathrm{C/Pt})/\rho_{\mathrm{C}} + \alpha(M_{\mathrm{Ru}}/M_{\mathrm{Pt}})/\rho_{\mathrm{Ru}} + 1/3\rho_{\mathrm{N}}\} \quad (15)$$

where m_{Pt} is the platinum loading of the catalyst layer and ρ_{Pt}, ρ_{Ru}, ρ_{C} and ρ_{N} are the bulk densities of Pt, Ru, C and Nafion. As $\alpha(M_{\mathrm{Ru}}/M_{\mathrm{Pt}})/\rho_{\mathrm{Ru}}$ is negligible with respect to $(\mathrm{C/Pt})/\rho_{\mathrm{C}}$ we can write:

$$d = d_0 + k(\mathrm{C/Pt}) \quad (16)$$

where d_0 is the thickness of the catalyst layer with unsupported Pt catalyst, and k is a constant, at a fixed Pt loading m_{Pt}. From this relation it is evident that the thickness of the catalyst layer linearly depends on the carbon amount.

PEM fuel cell performance for H_2 and H_2 + CO

Current-voltage curves for H_2 op and CO op at 70 °C and 90 °C for the different anodes are shown in Figs. 11 and 12. Cell performance at a current density of 0.5 A cm^{-2} is summarized in Table 4. As shown in these figures and table, PtRu/C catalysts showed a better CO tolerance than Pt/C. In Fig. 13 we can see the dependence of cell voltage at 0.5 A cm^{-2} on the carbon content of the catalyst layer for PtRu samples of various compositions. The values of the voltage at the lowest carbon content are due to the sample with Pt:Ru = 1:1

Table 4 Cell voltage (mV) at a current density of 0.5 A cm^{-2} for various anodes in different operating conditions. The Pt loading for all Ru-containing anodes was 0.6 mg cm^{-2}

Sample	70 °C H_2 op	70 °C CO op	90 °C H_2 op	90 °C CO op
20%, Pt (0.1 mg cm^{-2})	636	105	672	205
20%, PtRu = 3:1	630	204	657	476
20%, PtRu = 7:3	610	136	650	436
20%, PtRu = 1:1	592	413	621	557
20%, PtRu = 1:3	350	89	626	529
40%, PtRu = 1:1	649	415	674	611

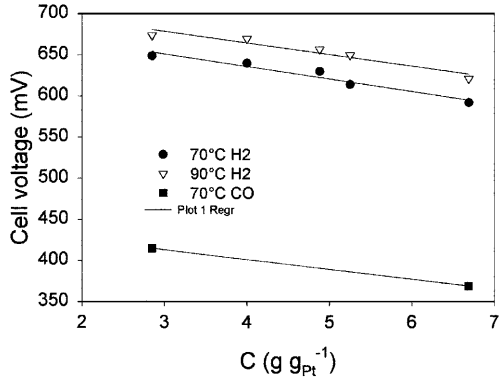

Fig. 13 Cell voltage at 0.5 A cm^{-2} versus carbon content of the catalyst layer at various conditions

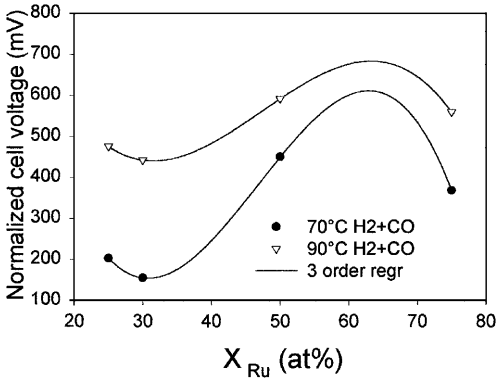

Fig. 15 Normalized cell voltage at 0.5 A cm^{-2} in CO op versus Ru content of PtRu/C catalysts

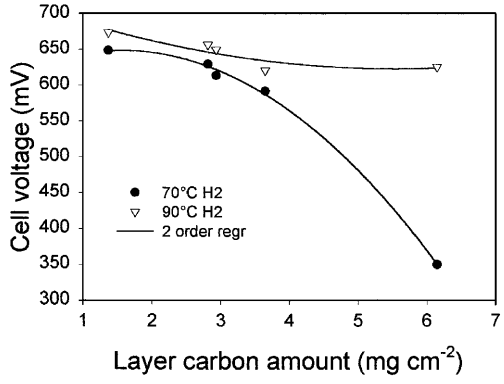

Fig. 14 Cell voltage at 0.5 A cm^{-2} in H_2 op at 70 and 90 °C versus carbon content of the catalyst layer comprising the value of PtRu/C with the highest carbon content (Pt:Ru = 1:3)

with Me/C = 40%; the other values are related to Me/C = 20% catalysts with different Ru content in the samples. A linear dependence of the voltage (loss of 20–26 mV per mg C) on the carbon amount, and then on the thickness of the catalyst layer, was revealed for the PtRu/C samples tested in H_2 op and the same dependence on carbon content was noted for the samples with Pt:Ru = 1:1 with Me/C = 20% and 40% tested in CO op. The increase of the catalyst thickness layer gives rise to an increase of electrode resistance. The Pt:Ru = 1:3 sample showed an anomalously high decrease of the voltage when tested at 70 °C in H_2, as shown in Fig. 14. This behaviour is probably related to the difficulty of the reactant gas reaching the inner Pt sites. At 90 °C, Pt:Ru = 1:3 also shows a linear dependence on the amount of carbon layer, as the higher mobility of H_2 at higher temperature allows the molecules to reach the inner Pt particles. In order to evaluate the net ruthenium effect, we have normalized the voltage of the PtRu samples in CO op with respect to the thickness effect as:

$$V_{CO^n} = V_{CO} + \Delta V_H \quad (17)$$

where ΔV_H is the voltage loss for H_2 in the PtRu samples with respect to the composition Pt:Ru = 3:1, related to the different carbon content of the catalyst layer. Figure 15 shows the V_{CO^n} versus Ru plot for PtRu anodes: at both 70 and 90 °C, by a three-order regression of experimental values, a sigmoidal curve was obtained with a maximum for 0.63 at% Ru. Taking into account that, for high Ru/Pt atomic ratios, part of the Ru is in the fcc PtRu alloy and part in the hcp PtRu alloy, probably this value is related to the maximum number of Pt-Ru pairs. As can be seen in Fig. 15, at 70 °C the width of the corrected cell voltage range is wider than 300 mV, while at 90 °C the range of V_{CO^n} values is less than 100 mV. At 90 °C, CO is less adsorbed onto the catalyst than at 70 °C, so at the higher temperature the effect of Ru content in the sample on cell performance is less visible.

Conclusions

1. The metal-support interactions affect the morphological characteristics of PtRu/C catalysts.
2. Pt-C interactions are stronger in the presence of Ru.
3. Pt-C and Ru-C interactions hinder the formation of Pt-Ru alloy.
4. PtRu compositions give rise to the formation of smaller Me particles than pure Pt and Ru.
5. The intercrystallite distance decreases with Ru content.
6. These morphological variations do not affect the performance of H_2 in a PEM fuel cell electrode. The only effect is related to the dilution of Pt atoms with respect to C, at a fixed Me/C ratio.
7. For CO + H_2 the formation of two solid solutions, fcc and hcp, shifts the maximum performance of the PtRu/C catalysts, obtained by a three-order regression of experimental values, towards a value of nominal Ru atomic fraction higher than 0.5. Therefore, in the presence of CO, the use of PtRu/C catalysts with nominal Pt:Ru compositions in the range 1:1–1:3 is recommended.

References

1. Schmidt VM, Brockerhoff P, Hohlein B, Menzer R, Stimming U (1994) J Power Sources 49: 229
2. Lemons RA (1990) J Power Sources 29: 251
3. Gasteiger HA, Markovich NM, Ross PN (1995) J Phys Chem 99: 16757
4. Berbeek H, Sachtler W (1976) J Catal 42: 257
5. Wang SR, Fedkiw PS (1992) J Electrochem Soc 139: 3151
6. Bittins-Cattaneo B, Iwasita T (1987) J Electroanal Chem 238: 151
7. Watanabe M, Motoo S (1975) J Electroanal Chem 60: 267
8. Miura H, Gonzales R (1982) J Phys Chem 86: 1577
9. Alerasool S, Gonzales R (1990) J Catal 124: 204
10. Franaszczuk K, Sobkowski J (1992) J Electroanal Chem 327: 235
11. Grgur B, Zhuang G, Markovic N, Ross PJ (1997) J Phys Chem B 101: 3910
12. Grgur B, Zhuang G, Markovic N, Ross PJ (1998) J Phys Chem B 102: 2494
13. Oetjen H-F, Schmidt VM, Stimming U, Trila F (1996) J Electrochem Soc 143: 3838
14. Wolohan P, Mitchell PCH, Thompsett D, Cooper SJ (1997) J Mol Catal A 119: 223
15. Iwasita T, Dalbeck R, Pastor E, Xia X (1994) Electrochim Acta 11/12: 1817
16. Gasteiger HA, Markovic N, Ross PN, Cairns EJ (1994) Electrochim Acta 11/12: 1825
17. Ianniello R, Schmidt VM, Stimming U, Stumper J, Wallau A (1994) Electrochim Acta 11/12: 1863
18. Gasteiger HA, Markovic N, Ross PN, Cairns EJ (1994) J Phys Chem 98: 617
19. Ehrburger P, Walker PL (1978) J Catal 55: 63
20. Rodriguez Reinoso F, Moreno Castilla C, Guerrero-Ruiz A, Rodriguez Ramos I, Lopez Gonzalez JD (1985) Appl Catal 15: 293
21. Torre T, Aricò AS, Alderucci V, Antonucci V, Giordano N (1994) Appl Catal A 114: 257
22. Trimm DL (1981) In: Bond GC (ed) Catalysis, vol 4. (Specialist periodical reports) Royal Society of Chemistry, London, p 210
23. van Dam HE, van Bekkum H (1991) J Catal 131: 335
24. Torres GC, Jablonski EL, Baronetti GT, Castro AA, de Miguel SR, Scelza OA, Blanco MD, Pena Jimenez MA, Fierro JLG (1997) Appl Catal A 161: 213
25. Roman-Martinez MC, Cazorla-Amoros D, Linares-Solano A, Salinas-Martinez de Lecea C, Yamashita H, Anpo M (1995) Carbon 33: 3
26. Rauhe BR, McLarnon FR, Cairns EJ (1995) J Electrochem Soc 142: 1073
27. He C, Kunz HR, Fenton JM (1997) J Electrochem Soc 144: 970
28. McBreen J, Mukerjee S (1995) J Electrochem Soc 142: 3399
29. Radmilovic V, Gasteiger HA, Ross PN (1995) J Catal 154: 98
30. Antolini E, Giorgi L, Pozio A, Passalacqua E (1999) J Power Sources 77: 136
31. Pearson's Crystallographic Data (1972), vol 16, p 8
32. Chu D, Gilman S (1996) J Electrochem Soc 143: 1686
33. Hadzi-Jordanov S, Angerstein-Kozlowska H, Vukovic M, Conway BE (1977) J Phys Chem 81: 2271
34. Watanabe M, Stonehart P (1988) Chem Lett 1497
35. Watanabe M, Sei H, Stonehart P (1989) J Electroanal Chem 261: 375
36. Vedrine JC, Dufaux M, Naccache C, Imelik B (1978) J Chem Soc Faraday Trans 74: 440
37. Shukla AK, Ravikumar MK, Roy A, Barman SR, Sarma DD, Aricò AS, Antonucci V, Pino L, Giordano N (1994) J Electrochem Soc 141: 1517
38. Biloul A, Coowar F, Contamin O, Scarbeck G, Savy M, van den Ham D, Riga J, Verbist J (1990) J Electroanal Chem 289: 189
39. Mittal KL (1976) J Vac Sci Technol 13: 19
40. Mason MG, Gerenser LG, Lee ST (1977) Phys Rev Lett 39: 288
41. Mason MG (1983) Phys Rev B 27: 748
42. Cheung TTP (1984) Surf Sci 140: 151
43. Eberhardt W, Fayet P, Cox DM, Fu Z, Kaldor A, Sherwood R, Sondericker D (1990) Phys Rev Lett 64: 780
44. Shukla AK, Aricò AS, El-Kathib KM, Kim H, Antonucci PL, Antonucci V (1999) Appl Surf Sci 137: 20
45. Denis MC, Lalande G, Guay D, Dodelet JP, Schulz R (1999) J Appl Electrochem 29: 951